Analysis of Interacting Cracks Using the Generalized Finite Element Method with Global-Local Enrichment Functions*

Dae-Jin Kim, Carlos Armando Duarte,† and Jeronymo Peixoto Pereira

Department of Civil and Environmental Engr.,

University of Illinois at Urbana-Champaign, Newmark Laboratory,

205 North Mathews Avenue, Urbana, Illinois 61801, USA

(Dated: January 9, 2008)

Abstract

This paper presents an analysis of interacting cracks using a generalized finite element method (GFEM) enriched with so-called global-local functions. In this approach, solutions of local boundary value problems computed in a global-local analysis are used to enrich the global approximation space through the partition of unity framework used in the GFEM. This approach is related to the global-local procedure in the FEM, which is broadly used in industry to analyze fracture mechanics problems in complex three-dimensional geometries. In this paper, we compare the effectiveness of the global-local FEM with the GFEM with global-local enrichment functions. Numerical experiments demonstrate that the latter is much more robust than the former. In particular, the GFEM is less sensitive to the quality of boundary conditions applied to the local problems than the global-local FEM. Stress intensity factors computed with the conventional global-local approach showed errors of up to one order of magnitude larger than in the case of the GFEM. The numerical experiments also demonstrate that the GFEM can account for interactions among cracks with different scale sizes, even when not all cracks are modeled in the global domain.

*Dedicated to Professor Fazil Erdogan for his seminal contributions to the analysis of fracture mechanics problems.

†Corresponding author.; e-mail: caduarte@uiuc.edu

I. INTRODUCTION

Three-dimensional interacting cracks appear in many practical engineering problems. Examples include corrosion-assisted cracks, multi-site damage analysis of lap joints and thermal fatigue cracks in cooling systems of nuclear power plants [1–4]. This class of problems is difficult to analyze due to the singularities at crack fronts and the complex stress distribution caused by the interaction of many cracks. The situation gets even more challenging when cracks with different scale sizes are involved, like in the case of macrocracks interacting with many microcracks. Small microcracks cannot be modeled by a global mesh designed to capture macrocracks. To handle this problem, the finite element method (FEM) requires extreme local refinements around the front of macrocracks and in regions where microcracks are located, leading to a high computational cost, especially in the three-dimensional case.

The global-local or sub-modeling procedure in the FEM [5–7] is an alternative to analyze interacting cracks. However, this approach is known to be sensitive to the quality of boundary conditions used in the local domains (sub-models) [7]. Accurate local solutions require the use of sufficiently large local domains and, in some cases, modeling of interacting features, like cracks, in the global problem. This leads to a large number of degrees of freedom in both global and local domains, and offsets some of the advantages of the procedure.

In this paper, we demonstrate that interacting cracks can be efficiently analyzed using the so-called generalized finite element method (GFEM) with global-local enrichment functions [8, 9]. In this procedure, local solutions computed in a global-local analysis are used to enrich the global solution space through the partition of unity framework used in the GFEM. The local solution enrichments are hierarchical and used only at a few nodes in the coarse global mesh. As a result, the enriched global problem can be solved at a low computational cost [9]. We also show that interactions among several cracks with different scale sizes can be accurately captured using the GFEM with global-local enrichment functions. The quality of the numerical solutions is measured using analytical solutions derived by Civelek and Erdogan [10] for the problem of an infinite strip containing multiple cracks.

The outline of this paper is as follows. The global-local FEM is briefly reviewed in Section II. The GFEM with global-local enrichment functions is summarized in Section III. Numerical

experiments comparing the global-local FEM and the GFEM with global-local enrichments are presented in Section IV. Section V draws the main conclusions from this investigation.

II. THE GLOBAL-LOCAL APPROACH IN THE FINITE ELEMENT METHOD

The global-local approach in the finite element method has a long history whose origin can be traced to the 1960's. It has also been called *zooming technique* or *sub-modeling* [5, 6]. This technique has been extensively used in industry although it is rarely mentioned in academic textbooks [5]. More recently, this approach has begun to be incorporated into parallel processing algorithms [11].

As an example to illustrate the approach, let us consider a structural part with a planar crack surface shown in Figure 1. The boundary conditions and geometric description of the crack surface are represented in Figure 1(a). The global-local FEM procedure involves two steps [5, 6]. First, the solution of the problem is computed on a coarse, global, quasi-uniform mesh like that shown in Figure 1(a). No mesh refinement around local features, like crack surfaces, is usually performed. Next, small sub-domains containing local features are extracted from the global domain and analyzed using the global solution as boundary conditions [5, 6]. Local domains are typically analyzed using very refined meshes like the one shown in Figure 1(b). The use of the crude global solution as boundary conditions for local problems is a key point in the procedure. Either displacement (Dirichlet) or traction (Neumann) boundary conditions can be used [5].

The computational cost of factorizing a matrix grows faster than linearly with respect to problem size. Therefore, by solving the global problem on a coarse mesh, and local problems on fine meshes, instead of refining the global mesh, the global-local FEM can significantly reduce computational costs when applied to large practical engineering problems.

In the procedure described above, the crack was discretized in the (coarse) global mesh. This may be difficult when the geometry of the domain is complex, when the crack is small, or when the analysis of several crack locations and configurations is required. Therefore, in engineering applications of the global-local FEM, local features like cracks are often not discretized in the global mesh and the global problem is solved as if there were no cracks in the domain. The cracks are modeled *only* in the local domains [5, 7]. This significantly reduces mesh generation efforts

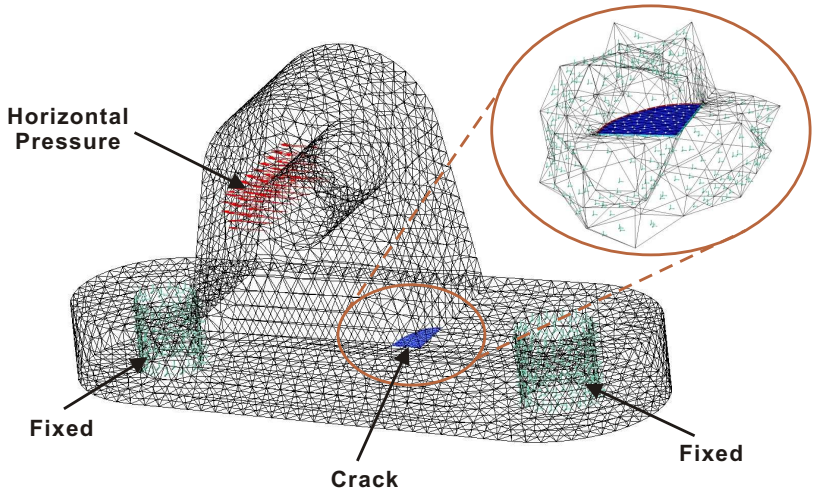

(a)Global analysis with a coarse mesh to provide boundary conditions for the extracted local domain.

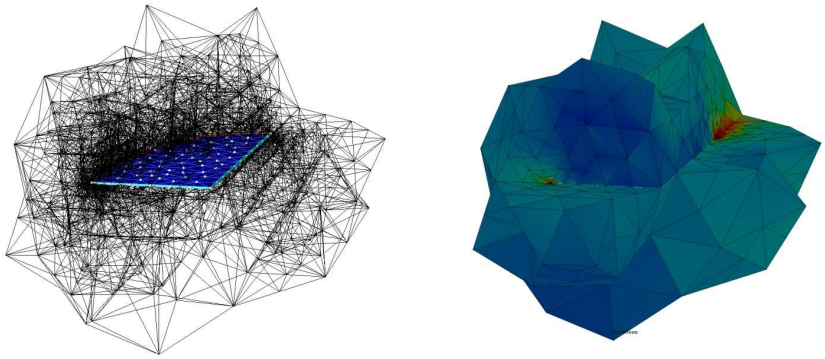

(b)Refined local problem and its solution.

FIG. 1: Global-local analysis for a structural component with a planar crack surface.

and enables the use of a single global solution for the analysis of any configuration of cracks in the domain. However, as demonstrated later in Section IV A 2, this approach may lead to large errors in the solution of the local problems.

An important issue for the global-local FEM is the size of local domains. The basic assumption of this approach is that the global solution is sufficiently accurate at the boundary of a local domain, or that the local domain is large enough such that a crude boundary condition does not affect the quality of the local solution. It is not always easy to comply with this assumption since

local problems are modeled in the neighborhood of local features such as cracks and cutouts where the solution exhibits strong gradients or singularities. In addition, the well known pollution effect may cause the propagation of *discretization* errors over large distance in a domain [12]. For crack problems, it is usually recommended that the size of a sub-domain be at least 2.5 to 3 times larger than the length of the crack [7]. This may require, for example, the inclusion of more than one crack in a local domain leading to large local problems and to difficulties in generating appropriate meshes in the local domains.

III. THE GENERALIZED FINITE ELEMENT METHOD WITH GLOBAL-LOCAL ENRICHMENT FUNCTIONS

This section describes the basic concepts of the generalized finite element method (GFEM) and the construction of enrichment functions using a procedure similar to that employed in the global-local FEM. The main features of these so-called global-local enrichment functions are discussed. We also compare the global-local FEM with the GFEM enriched with global-local functions.

A. The Generalized Finite Element Method

The construction of generalized finite element approximations is briefly reviewed in this section. Further details can be found in, for example, [13–17].

A shape functions, $\phi_{\alpha i}$, in the GFEM is built from the product of a linear finite element shape function, φ_α, and an enrichment function, $L_{\alpha i}$,

$$\phi_{\alpha i}(\boldsymbol{x}) = \varphi_\alpha(\boldsymbol{x}) L_{\alpha i}(\boldsymbol{x}) \qquad (\text{no summation on } \alpha) \tag{1}$$

where α is a node in the finite element mesh. Figure 2 illustrates the construction of GFEM shape functions. The linear finite element shape functions $\varphi_\alpha,\ \alpha = 1,\ldots,N$, in a finite element mesh with N nodes constitute a partition of unity, i.e., $\sum_{\alpha=1}^{N} \varphi_\alpha(\boldsymbol{x}) = 1$ for all $\boldsymbol{x}$ in a domain Ω covered by the finite element mesh. This is a key property used in partition of unity methods like the GFEM. Linear combination of the GFEM shape functions $\phi_{\alpha i},\ \alpha = 1,\ldots,N$, can represent *exactly* any enrichment function $L_{\alpha i}$.

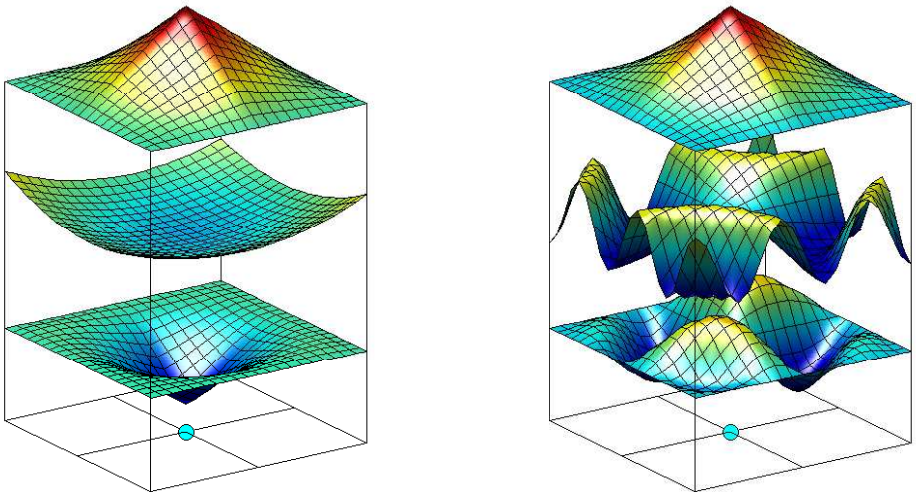

(a) (b)

FIG. 2: Construction of a generalized FEM shape function using a polynomial (a) and a non-polynomial enrichment (b). Here, φ_α are the functions at the top, the enrichment functions, $L_{\alpha i}$, are the functions in the middle, and the generalized FE shape functions, $\phi_{\alpha i}$, are the resulting bottom functions.

Several enrichment functions can be hierarchically added to any node α in a finite element mesh. Thus, if $m(\alpha)$ is the number of enrichment functions at node α, the GFEM approximation, u_{hp}, of a function u can be written as

$$u_{hp}(\boldsymbol{x}) = \sum_{\alpha=1}^{N} \sum_{i=1}^{m(\alpha)} a_{\alpha i} \phi_{\alpha i}(\boldsymbol{x}) = \sum_{\alpha=1}^{N} \sum_{i=1}^{m(\alpha)} a_{\alpha i} \varphi_\alpha(\boldsymbol{x}) L_{\alpha i}(\boldsymbol{x})$$

The main strength of the generalized FEM is its ability to use non-polynomial enrichment functions as illustrated in Figure 2(b). Expansions of the elasticity solution in the neighborhood of a crack (Westergaard functions) can be taken as enrichment functions at nodes near a crack front [14, 18–22]. Discontinuities in a displacement field can be approximated independently of the underlying finite element mesh if Heaviside functions are used as enrichment functions [21–25]. Custom-built enrichment functions that are solutions of local boundary value problems can be used as well [8, 9, 26]. These so-called global-local enrichment functions are described in detail in Section III B.

B. A Global-Local Approach to Build Enrichment Functions

In this section, we review a global-local approach to build enrichment functions for the generalized FEM. Additional details can be found in [8, 9]. We focus on three-dimensional linear elasticity problems. The formulation is, however, applicable to other classes of problems as well.

1. Formulation of Global Problem

Consider the domain $\bar{\Omega}_G = \Omega_G \cup \partial\Omega_G \subset \boldsymbol{R}^3$ illustrated in Figure 3(a). The boundary is decomposed as $\partial\Omega_G = \partial\Omega_G^u \cup \partial\Omega_G^\sigma$ with $\partial\Omega_G^u \cap \partial\Omega_G^\sigma = \emptyset$.

The strong form of the equilibrium and constitutive equations is given by

$$\nabla \cdot \boldsymbol{\sigma} = \boldsymbol{0} \qquad \boldsymbol{\sigma} = \boldsymbol{C} : \boldsymbol{\varepsilon} \qquad \text{in } \Omega_G, \tag{2}$$

where $\boldsymbol{C}$ is Hooke's tensor. The following boundary conditions are prescribed on $\partial\Omega_G$

$$\boldsymbol{u} = \bar{\boldsymbol{u}} \text{ on } \partial\Omega_G^u \qquad \boldsymbol{\sigma} \cdot \boldsymbol{n} = \bar{\boldsymbol{t}} \text{ on } \partial\Omega_G^\sigma, \tag{3}$$

where $\boldsymbol{n}$ is the outward unit normal vector to $\partial\Omega_G^\sigma$, and $\bar{\boldsymbol{t}}$ and $\bar{\boldsymbol{u}}$ are prescribed tractions and displacements, respectively.

Let $\boldsymbol{u}_G^0$ denote a generalized FEM approximation of the solution $\boldsymbol{u}$ of problem (2), (3). The approximation $\boldsymbol{u}_G^0$ is the solution of the following problem:

Find $\boldsymbol{u}_G^0 \in \boldsymbol{X}_G^{hp}(\Omega_G) \subset H^1(\Omega_G)$ such that $\forall\, \boldsymbol{v}_G^0 \in \boldsymbol{X}_G^{hp}(\Omega_G)$

$$\int_{\Omega_G} \boldsymbol{\sigma}(\boldsymbol{u}_G^0) : \boldsymbol{\varepsilon}(\boldsymbol{v}_G^0) d\boldsymbol{x} + \eta \int_{\partial\Omega_G^u} \boldsymbol{u}_G^0 \cdot \boldsymbol{v}_G^0 d\boldsymbol{s} = \int_{\partial\Omega_G^\sigma} \bar{\boldsymbol{t}} \cdot \boldsymbol{v}_G^0 d\boldsymbol{s} + \eta \int_{\partial\Omega_G^u} \bar{\boldsymbol{u}} \cdot \boldsymbol{v}_G^0 d\boldsymbol{s} \tag{4}$$

where $\boldsymbol{X}_G^{hp}(\Omega_G)$ is a discretization of the Hilbert space $H^1(\Omega_G)$ built with generalized FEM shape functions, and η is a penalty parameter. Problem (4) leads to a system of linear equations for the unknown degrees of freedom of $\boldsymbol{u}_G^0$. The mesh used to solve problem (4) is typically a coarse quasi-uniform mesh. This problem is analogous to the first step of the global-local FEM presented in Figure 1(a) and denoted hereafter as *initial global problem*.

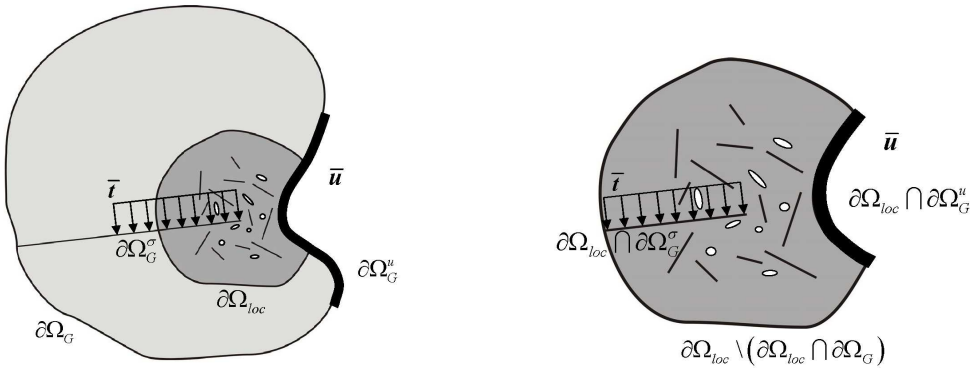

(a)A global domain containing one macrocrack and several microcracks.

(b)A local domain extracted from the global domain in the neighborhood of the macrocrack front.

FIG. 3: Notations for the GFEM with global-local enrichment functions.

2. Local Problems

Let Ω_{loc} denote a subdomain of Ω_G as shown in Figure 3(b). This local domain may contain cracks, holes, inclusions, fibers, or other local features of interest.

The following local problem is solved on Ω_{loc} after the global solution $\boldsymbol{u}_G^0$ is computed as described above:

Find $\boldsymbol{u}_{loc} \in \boldsymbol{X}_{loc}^{hp}(\Omega_{loc}) \subset H^1(\Omega_{loc})$ such that $\forall\, \boldsymbol{v}_{loc} \in \boldsymbol{X}_{loc}^{hp}(\Omega_{loc})$

$$\int_{\Omega_{loc}} \boldsymbol{\sigma}(\boldsymbol{u}_{loc}) : \boldsymbol{\varepsilon}(\boldsymbol{v}_{loc}) d\boldsymbol{x} + \eta \int_{\partial\Omega_{loc} \setminus (\partial\Omega_{loc} \cap \partial\Omega_G^{\sigma})} \boldsymbol{u}_{loc} \cdot \boldsymbol{v}_{loc} d\boldsymbol{s} =$$
$$\eta \int_{\partial\Omega_{loc} \setminus (\partial\Omega_{loc} \cap \partial\Omega_G)} \boldsymbol{u}_G^0 \cdot \boldsymbol{v}_{loc} d\boldsymbol{s} + \eta \int_{\partial\Omega_{loc} \cap \partial\Omega_G^{u}} \bar{\boldsymbol{u}} \cdot \boldsymbol{v}_{loc} d\boldsymbol{s} + \int_{\partial\Omega_{loc} \cap \partial\Omega_G^{\sigma}} \bar{\boldsymbol{t}} \cdot \boldsymbol{v}_{loc} d\boldsymbol{s} \qquad (5)$$

where $\boldsymbol{X}_{loc}^{hp}(\Omega_{loc})$ is a discretization of $H^1(\Omega_{loc})$ using GFEM shape functions.

A key aspect of problem (5) is the use of the generalized FEM solution of the global problem, $\boldsymbol{u}_G^0$, as boundary condition on $\partial\Omega_{loc} \setminus (\partial\Omega_{loc} \cap \partial\Omega_G)$. Exact boundary conditions are prescribed on portions of $\partial\Omega_{loc}$ that intersect either $\partial\Omega_G^{u}$ or $\partial\Omega_G^{\sigma}$. This problem is analogous to the second step of the global-local FEM presented in Figure 1(b) and denoted hereafter as *local problem*.

3. Global-Local Enrichment Functions

The error in the local solution $\boldsymbol{u}_{loc}$ depends not only on the discretization used in the local domain Ω_{loc}, but, more importantly, also on the quality of boundary conditions used on $\partial\Omega_{loc}\backslash(\partial\Omega_{loc}\cap\partial\Omega_G)$, i.e. $\boldsymbol{u}_G^0$. In the GFEM proposed in [8, 9], this issue is addressed by going one step further in a global-local analysis; *the local solution $\boldsymbol{u}_{loc}$ is used as an enrichment function for the global problem.* The local solution is called a *global-local enrichment function* and is used to define the following vector-valued global shape function

$$\boldsymbol{\phi}_\alpha = \varphi_\alpha \boldsymbol{u}_{loc} \tag{6}$$

where φ_α denotes a partition of unity function defined in the coarse *global* mesh used to solve the global problem presented in Section III B 1. This function is used at nodes $\boldsymbol{x}_\alpha$ of the global mesh whose support, ω_α, is contained in the local domain Ω_{loc}. In our implementation, we enrich each component of the displacement vector with the corresponding component of the local solution $\boldsymbol{u}_{loc}$. Thus, a global-local enrichment adds three degrees of freedom to a node when solving a three-dimensional elasticity problem. The global problem defined in Section III B 1 is then solved again using these global functions. The solution of this enriched global problem is denoted by $\boldsymbol{u}_G^E$. This problem is denoted hereafter as *enriched global problem*. In [9], we demonstrated how this problem can be efficiently solved using the solution of the initial global problem.

The GFEM with global-local enrichment functions can account for possible interactions of local (near crack, for example) and global (structural) behavior. This procedure also addresses the loss of accuracy in the local solution caused by the crude boundary conditions used in the local domain. Roughly speaking, this can be explained by the fact that the global partition of unity φ_α, and therefore $\boldsymbol{\phi}_\alpha$, are zero at the boundary of local domain Ω_{loc}, where the accuracy of $\boldsymbol{u}_{loc}$ is more severely affected by the boundary conditions applied at $\partial\Omega_{loc}$. The enrichment of the global mesh with the local solution is illustrated in Figure 4 using the same example introduced in Section II. Hereafter, *GFEM*$^{\text{g-l}}$ denotes the GFEM with global-local enrichment functions.

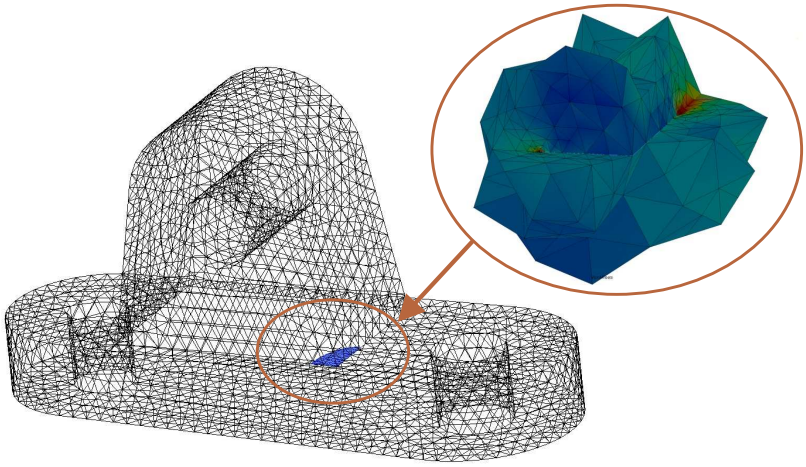

FIG. 4: Enrichment of the coarse global mesh with a local solution.

IV. NUMERICAL EXPERIMENTS

In this section, we analyze the performance of the *GFEM*$^{\text{g-l}}$ in the analysis of interacting cracks. We compare the quality of stress intensity factors extracted from the solution of the enriched global problem, $\boldsymbol{u}_G^E$, with those extracted from the local solution, $\boldsymbol{u}_{loc}$.

The local solution $\boldsymbol{u}_{loc}$ is computed using the generalized finite element method described in Section III A. This enables us to solve the local problems using meshes that do not fit the crack surfaces, as required in the FEM. Therefore, strictly speaking, $\boldsymbol{u}_{loc}$ is computed using a global-local GFEM and not a global-local FEM. However, these methods suffer from the same limitations, and it is reasonable to assume that the conclusions drawn here are also valid for the global-local FEM. Hereafter, the procedure used to compute $\boldsymbol{u}_{loc}$ is denoted by *GL-FEM*.

The numerical examples presented below include an analysis of interacting cracks, an inclined crack and cracks with different scale sizes. The main focus of the numerical experiments is on how the quality of boundary conditions for the local problems affects that of the stress intensity factors extracted from *GFEM*$^{\text{g-l}}$ and *GL-FEM* solutions. The numerical experiments show that the *GFEM*$^{\text{g-l}}$ is much less sensitive to the quality of local boundary conditions and provides more accurate stress intensity factors than the *GL-FEM*.

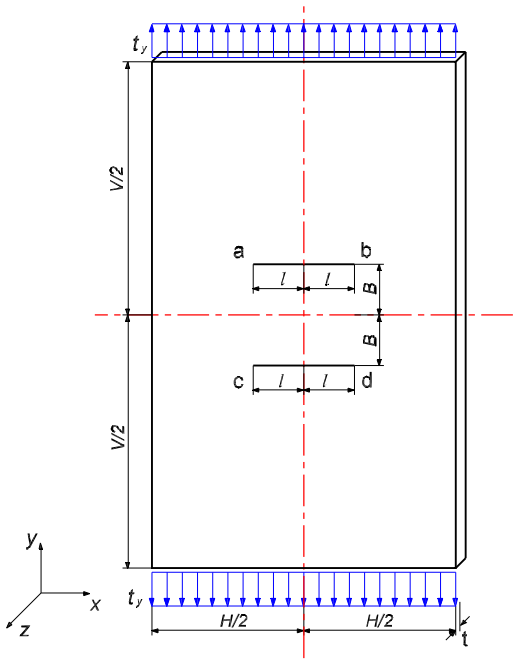

FIG. 5: Description of a problem with two interacting cracks in an infinite strip.

A. Analysis of Two Interacting Macrocracks

An example with two interacting cracks in an infinite strip is considered in this section. The problem is illustrated in Figure 5. The general plane elastic problem of an infinite strip containing multiple cracks perpendicular to its boundary was analysized by Civelek and Erdogan [10]. They showed that for the configuration shown in Figure 5, the interaction between the cracks produces a nonzero mode-two stress intensity factor, K_{II}. This leads to the propagation of the cracks away from each other. This effect becomes more significant as the distance between the cracks decreases [10]. In this section, we investigate how well the *GFEM*$^{\text{g-l}}$ and the *GL-FEM* can captute the interaction between the two cracks as B/H goes to zero (Cf. Figure 5). The stress intensity factors are extracted from $\boldsymbol{u}_G^E$ and $\boldsymbol{u}_{loc}$, respectively, as discussed above.

Three-dimensional tetrahedron elements are used in our computations. The Poisson's ratio is set to zero in order to minimize three-dimensional effects in the computed solution. This enables us to use Civelek and Erdogan's solution presented in [10] as a reference. The other parameters

assumed in our computations are as follows: Young's modulus $E = 200,000$; in-plane dimensions $H = 10.0$, $2l = 4.0$, $V = 200.0$; domain thickness $t = 1.0$; vertical traction $t_y = 100.0$. Since the vertical dimension is twenty times larger than the horizontal dimension, we can assume that the solution on this finite domain is very close to the case of an infinite strip.

The SIFs are extracted using the cut-off function method [27–29] and normalized as in [10] using

$$k_{I\ (II)} = \frac{K_{I\ (II)}}{t_y\sqrt{\pi l}} \tag{7}$$

where $k_{I\ (II)}$ denotes the normalized mode I (II) SIF, $K_{I\ (II)}$ denotes the original mode I (II) SIF, t_y is the traction applied at $y = \pm V/2$, and $2l$ is the crack length.

1. Analysis with Cracks Discretized in the Global Domain

The discretizations shown in Figure 6 are used in the analysis presented in this section. The global mesh is quite coarse, as shown in Figure 6(a), and has only one layer of elements in the out-of-plane direction. Heaviside enrichment functions are used to represent the cracks. This enables the cracks to cut elements in the mesh, as described in Section III A.

Four local problems are created, one for each crack front as illustrated in Figure 6(a). The local meshes are strongly refined in the neighborhood of the crack fronts. Westergaard functions are used in the elements intersecting the crack front. In the case of the *GL-FEM*, stress intensity factors are extracted from solutions computed in these local domains.

The local solutions are used to enrich nodes in the global mesh, as illustred in Figure 6(c). Only four nodes per crack front are enriched with these functions (two nodes at $z = 0$ and two at $z = t$). As a result, the enriched global problem has almost the same number of degrees of freedom as the initial global problem (Cf. Table I). In the case of the *GFEM*$^{\text{g-l}}$, stress intensity factors are extracted from the solution computed in this enriched global problem.

The polynomial order of the shape functions used in the initial and enriched global problems is $p = 1$, whereas cubic polynomial shape functions ($p = 3$) are used in the local problems. It should be emphasized that the interacting cracks *are discretized* in the global domain. This is in contrast to the analysis presented in Section IV A 2 where the cracks are not discretized in the global domain.

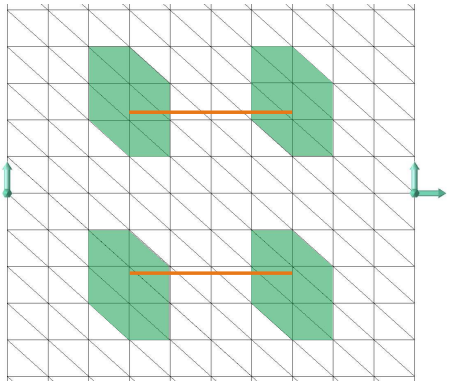

(a)Discretization of cracks in the initial global problem. The shaded areas represent the local domains extracted from the coarse global mesh.

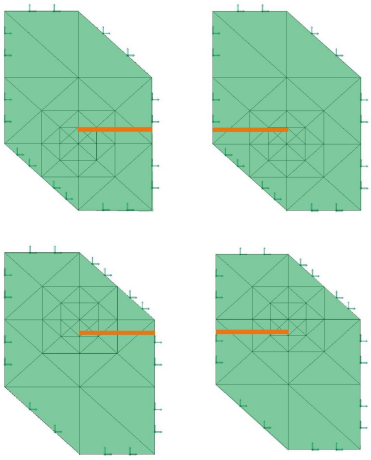

(b)Graded meshes used in the discretization of local problems.

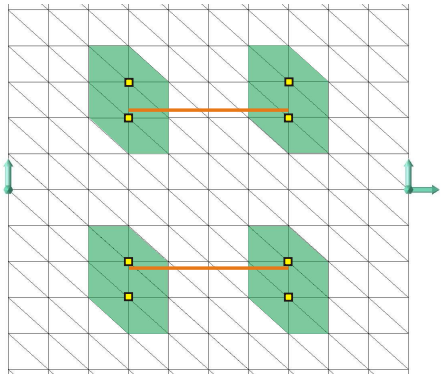

(c)Enrichment of global discretization with local solutions. Global nodes enriched with local solutions are represented with squares.

FIG. 6: Discretization of a problem with two interacting cracks using tetrahedral elements. Front view of the strip shown in Figure 5 for the case $B/H = 2$. Note that the cracks are discretized in the global domain and a three-dimensional discretization is used.

TABLE I: Mode I and II stress intensity factors for the problem shown in Figure 5, and cracks are discretized in the global domain. Global problems are solved with linear shape functions. Abbreviations nDOFs, IG, L and EG in the table represent the number of degrees of freedom, initial global, local and enriched global problems, respectively.

B/H	nDOFs	nDOFs	nDOFs	Normalized Mode I SIF			Normalized Mode II SIF		
	(IG)	(L)	(EG)	*GL-FEM*	*GFEM*$^{\text{g-l}}$	Ref.	*GL-FEM*	*GFEM*$^{\text{g-l}}$	Ref.
0.2	3438	18018	3486	0.7360	0.9254	0.9749	-0.0273	-0.0777	-0.0656
0.3	3438	19278	3486	0.7709	0.9758	1.0437	-0.0182	-0.0474	-0.0330
0.4	3438	17328	3486	0.7893	1.0072	1.0839	-0.0104	-0.0410	-0.0155
1.0	3438	19278	3486	0.7998	1.0445	1.1096			

Table I lists the computed (normalized) mode I and II SIFs (k_I and k_{II}) extracted from *GL-FEM* and *GFEM*$^{\text{g-l}}$ solutions. The reference values from Civelek and Erdogan [10] are also listed. Figure 7 plots the data from the table. The results show that mode I SIFs extracted from *GFEM*$^{\text{g-l}}$ solutions are much more accurate than those from *GL-FEM* solutions. For the case $B/H = 0.2$, the relative error of k_I extracted from the *GFEM*$^{\text{g-l}}$ solution is 5.08 %, whereas the error is 24.5 % in the case of the *GL-FEM*. The relative error in the computed k_I by *GL-FEM* is therefore almost five times larger than the one computed with the *GFEM*$^{\text{g-l}}$. A similar trend is observed for other values of B/H. Mode II SIFs are also listed in Table I for reference. However, since for this problem k_{II} is much smaller than k_I, it cannot be computed as accurately as k_I using either the *GL-FEM* or the *GFEM*$^{\text{g-l}}$. Thus, we do not use k_{II} as a basis for comparison of performance of the methods. This comparison is done instead in Section IV B.

As a subsequent analysis, we investigate the effect of the quality of boundary conditions used in local problems on the quality of the SIFs computed with the *GL-FEM* and *GFEM*$^{\text{g-l}}$. Two approaches are used to improve the quality of the boundary conditions. The global problem is solved with (i) cubic shape functions, (ii) cubic shape functions and Westergaard function enrichments at nodes of the global mesh close to the crack fronts (four nodes per crack front). The Westergaard enrichments are subsequently replaced by the local solutions in the enriched global

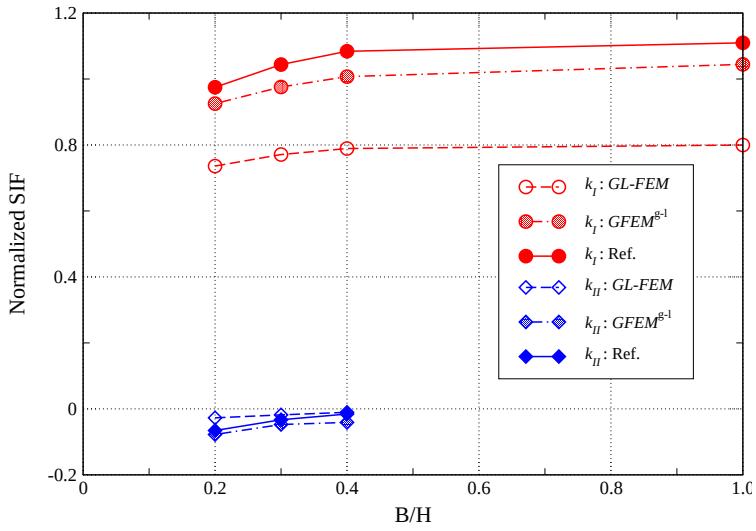

FIG. 7: Analysis with interacting cracks discretized in the global domain. Global problems are solved with linear shape functions. Ref. represents the reference SIF values obtained from [10].

problem as illustrated in Figure 6(c). All other parameters are the same as in the $p = 1$ case. The results for these two cases are presented in Figures 8 and 9. Table II lists the results for case (i). It is observed, as expected, that the stress intensity factors in the *GL-FEM* greatly improve as more accurate boundary conditions are used in the local problems. However, they are still significantly less accurate than those computed with the *GFEM*$^{g-l}$. The relative error of k_I extracted from *GFEM*$^{g-l}$ solutions is consistently below 0.5 % whereas it is about 10 % in the case of the *GL-FEM*.

The robustness of the *GFEM*$^{g-l}$ demonstrated in this example is an important advantage over the *GL-FEM* since in practice it is generally not possible to quantify the quality of the boundary conditions.

2. *Analysis with Cracks Not Discretized in the Global Domain*

As discussed in Section II, quite often in practical finite element simulations, local features like cracks are not discretized in the global problem. In this section, we perform the same analysis as in Section IV A 1 but the initial global problem is solved without any cracks in the domain. The problem shown in Figure 5 is solved using this approach along with the discretizations shown in

TABLE II: Mode I and II stress intensity factors for the problem shown in Figure 5, and cracks are discretized in the global domain. Global problems are solved with cubic shape functions.

B/H	nDOFs (IG)	nDOFs (L)	nDOFs (EG)	Mode I SIF			Mode II SIF		
				GL-FEM	*GFEM*$^{g\text{-}l}$	Ref.	*GL-FEM*	*GFEM*$^{g\text{-}l}$	Ref.
0.2	34380	18018	34428	0.8908	0.9771	0.9749	-0.0578	-0.0693	-0.0656
0.3	34380	19278	34428	0.9446	1.0436	1.0437	-0.0338	-0.0375	-0.0330
0.4	34380	17328	34428	0.9767	1.0803	1.0839	-0.0186	-0.0169	-0.0155
1.0	34380	19278	34428	1.0005	1.1135	1.1096			

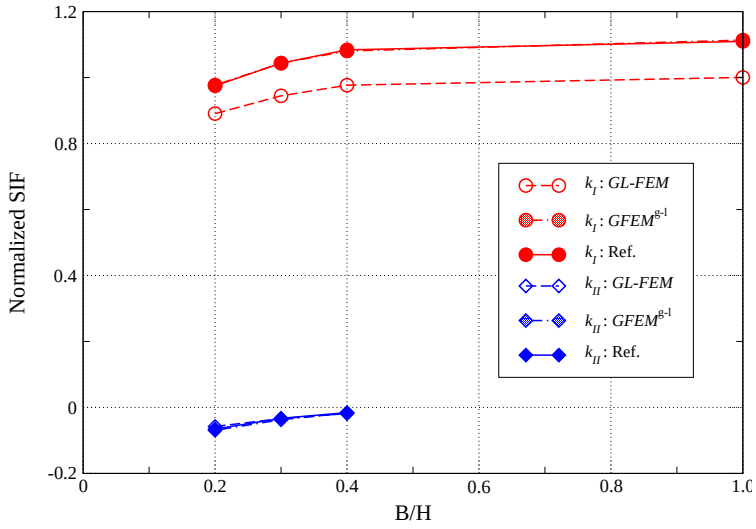

FIG. 8: Analysis with interacting cracks discretized in the global domain. Global problems are solved with cubic shape functions.

Figure 10. Only two local problems are created in this case, and each local problem includes the entire crack as illustrated in Figure 10(b). The cracks are described only in the local problems using Heaviside and Westergaard enrichment functions. The refinement level at the crack fronts is the same as in Section IV A 1. The local solutions are used to enrich nodes in the global mesh as illustrated in 10(c). Twenty nodes per crack are enriched in this case. It should be emphasized that the interacting cracks *are not discretized* in the global domain in contrast with the example

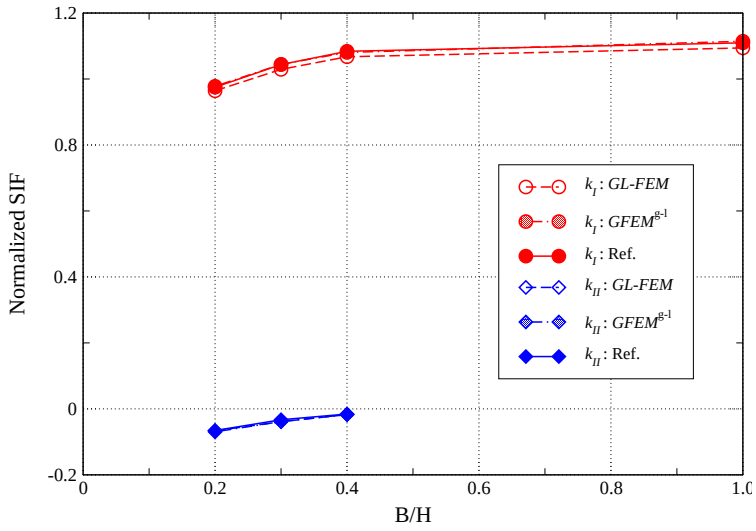

FIG. 9: Analysis with interacting cracks discretized in the global domain. Global problems are solved with cubic shape functions and Westergaard function enrichments.

analyzed in Section IV A 1.

The polynomial order of shape functions used in the initial and enriched global problems is set to $p = 1$, whereas cubic polynomial shape functions ($p = 3$) are used in the local problems. Table III lists the results for this case. Figure 11 plots the data from the table. The difference in quality of SIFs extracted from *GFEM*$^{g-l}$ and *GL-FEM* is even more significant than in the previous section. For example, the relative error in mode I SIF for $B/H = 0.2$ computed by the *GFEM*$^{g-l}$ is 4.05 %, whereas in the case of the *GL-FEM* it is 52.64 %. We can observe that the error in k_I computed with the *GL-FEM* is about twice as large as in the case reported in Table I. In contrast, the error in the case of the *GFEM*$^{g-l}$ is about the same as in Table I, in spite of the fact that the cracks were not modeled in the initial global problem.

As in the analysis presented in Section IV A 1, we investigate the effect of using cubic shape functions in the global problem. All other parameters are kept unchanged. The results for this choice of shape functions are presented in Figure 12 and in Table IV. Westergaard enrichments are not used in the global domain since in this domain the cracks are not discretized. It can be observed from Figure 12 and Table IV that the mode I SIFs computed with the *GL-FEM do not improve in this case*. This shows that if the cracks are not discretized in the global problem, the quality of boundary conditions used in the local problems may not improve even if higher order

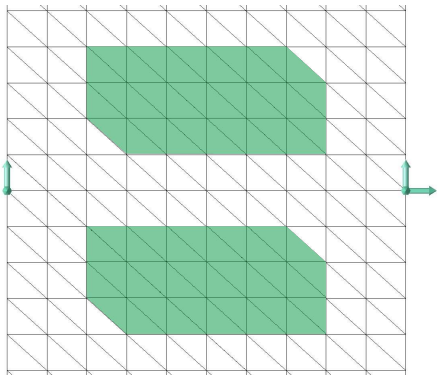

(a)The shaded areas represent the local domains extracted from the coarse global mesh.

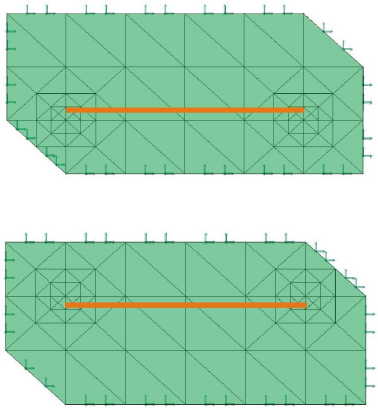

(b)Graded meshes used in the discretization of local problems.

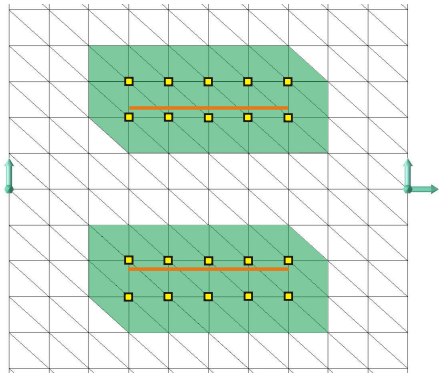

(c)Enrichment of global discretization with local solutions. Global nodes enriched with local solutions are represented with squares.

FIG. 10: Discretization of a problem with two interacting cracks. Front view for the case $B/H = 2$. The cracks are *not* discretized in the global domain.

elements or finer meshes are used in the global problem. The mode I SIFs in the *GFEM*$^{\text{g-l}}$ have an error of less than 1 % while in the case of the *GL-FEM* the error is about five times larger than those reported in Table II. This, again, shows that the *GFEM*$^{\text{g-l}}$ is more robust and can provide more accurate solutions than the *GL-FEM*, even in such an extreme situation where no

TABLE III: Mode I and II stress intensity factors for the problem shown in Figure 5. Cracks are not discretized in the global domain, and linear shape functions are used in the global domain.

B/H	nDOFs	nDOFs	nDOFs	Normalized Mode I SIF			Normalized Mode II SIF		
	(IG)	(L)	(EG)	*GL-FEM*	*GFEM*$^{g\text{-}l}$	Ref.	*GL-FEM*	*GFEM*$^{g\text{-}l}$	Ref.
0.2	3366	36708	3486	0.4617	0.9354	0.9749	-0.0270	-0.0906	-0.0656
0.3	3366	39228	3486	0.4625	0.9834	1.0437	-0.0162	-0.0537	-0.0330
0.4	3366	35328	3486	0.4630	0.9987	1.0839	-0.0043	-0.0103	-0.0155
1.0	3366	39228	3486	0.4604	1.0425	1.1096			

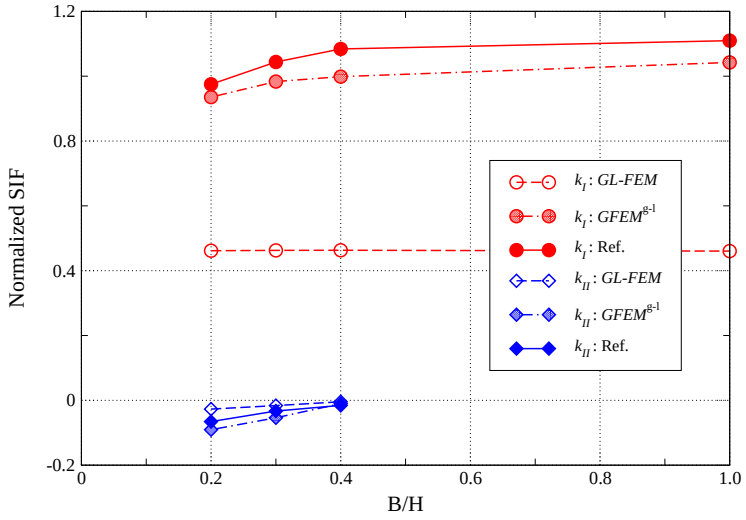

FIG. 11: Analysis with interacting cracks not discretized in the global domain. Global problems are solved with linear shape functions.

local features are represented in the global domain.

B. Analysis of an Inclined Crack

As a second example, we analyze the mixed-mode fracture problem shown in Figure 13. In contrast with the problem analyzed in Section IV A, here mode I and II stress intensity factors are of the same order magnitude. Thus, they can be extracted with the same level of accuracy. We

TABLE IV: Mode I and II stress intensity factors for the problem shown in Figure 5. Cracks are not discretized in the global domain and cubic shape functions are used in the global domain.

B/H	nDOFs (IG)	nDOFs (L)	nDOFs (EG)	Mode I SIF			Mode II SIF		
				GL-FEM	*GFEM*$^{g\text{-}l}$	Ref.	*GL-FEM*	*GFEM*$^{g\text{-}l}$	Ref.
0.2	33660	36708	33780	0.4617	0.9807	0.9749	-0.0270	-0.0720	-0.0656
0.3	33660	39228	33780	0.4625	1.0517	1.0437	-0.0162	-0.0459	-0.0330
0.4	33660	35328	33780	0.4630	1.0902	1.0839	-0.0043	-0.0186	-0.0155
1.0	33660	39228	33780	0.4604	1.1125	1.1096			

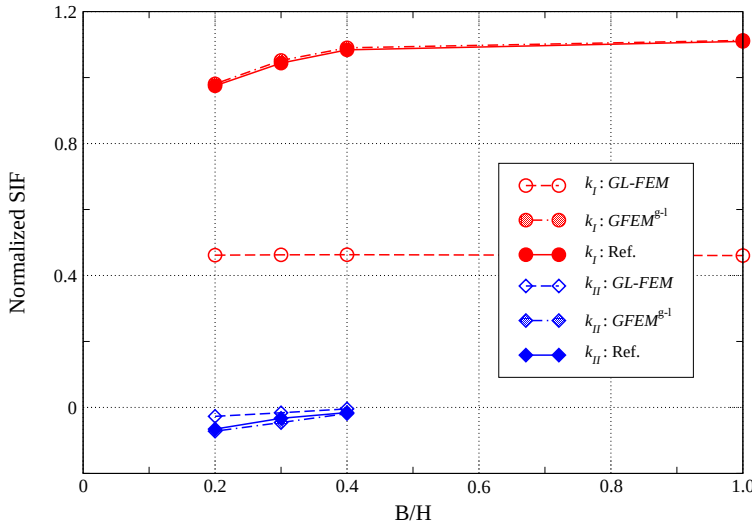

FIG. 12: Analysis with interacting cracks not discretized in the global domain. Global problems are solved with cubic shape functions.

compare SIFs extracted from *GL-FEM* and *GFEM*$^{g\text{-}l}$ solutions with reference values computed by Szabo and Babuška [27] using the p version of the finite element method with $p = 8$.

Three-dimensional tetrahedron elements are used in our computations as in Section IV A. The Poisson's ratio is set to zero to compare our results with the reference values computed assuming plane stress condition. The following parameters are also adopted in our simulation: Young's modulus $E = 1.0$; in-plane dimensions $w = 1.0$; domain thickness $t = 1.0$; vertical traction $t_y = 1.0$.

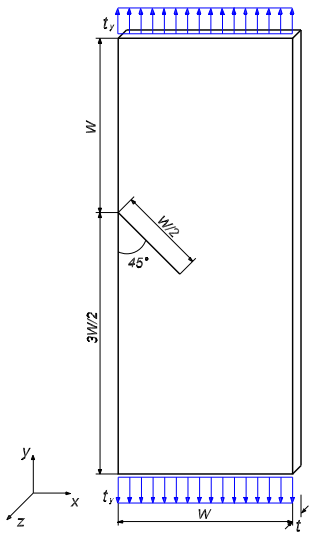

FIG. 13: Rectangular panel with a throught-the-thickness inclined crack.

The SIFs are extracted using the cut-off function method [27–29] and normalized using

$$k_{I\ (II)} = \frac{K_{I\ (II)}}{t_y\sqrt{2\pi w}} \tag{8}$$

where $k_{I\ (II)}$ denotes the normalized mode I (II) SIF.

The domain is discretized as shown in Figure 14. The global mesh is quite coarse, and only one layer of elements is used in the out-of-plane direction. The inclined crack is discretized only in the local domain, as in Section IV A 2, and is modeled using Heaviside and Westergaard functions. The local mesh is refined around the crack front to obtain accurate solutions, as in the previous section. In the case of *GFEM*$^{\text{g-l}}$, the local solutions are used to enrich eighteen nodes in the global mesh as illustrated in Figure 14(b). Quadratic shape functions are used in the global domain, and cubic shape functions in the local domain.

Table V lists normalized mode I and II stress intensity factors extracted from *GL-FEM* and *GFEM*$^{\text{g-l}}$ solutions. The reference values from Szabo and Babuška [27] are also listed. The relative error of k_I extracted from the *GFEM*$^{\text{g-l}}$ solution is 2.65 %, while it is 64.29 % in the case of *GL-FEM*. Thus, k_I computed with the *GL-FEM* has an error almost twenty-four times larger than the one computed with *GFEM*$^{\text{g-l}}$. This same level of accuracy is achieved by *GFEM*$^{\text{g-l}}$ in the case of k_{II}. The relative errors in mode II SIF are 3.21 % and 56.03 % in the *GFEM*$^{\text{g-l}}$

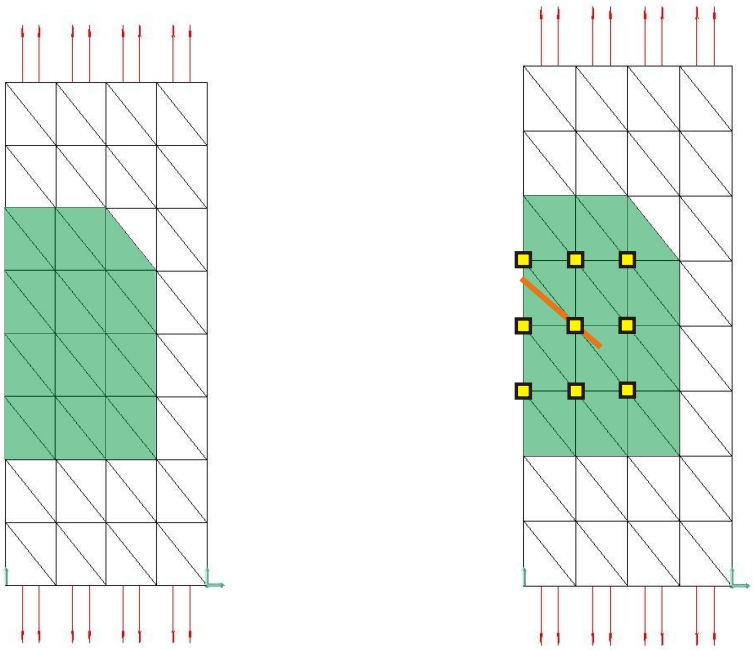

(a)The shaded areas represent the local domain extracted from the coarse global mesh.

(b)Enrichment of global discretization with local solutions. Global nodes enriched with local solutions are represented with squares.

FIG. 14: Discretization of the problem with an inclined crack. The cracks are *not* discretized in the global domain.

and *GL-FEM*, respectively. This result demonstrates that $GFEM^{g\text{-}l}$ can deliver much higher level of accuracy in the extraction of both mode I and II SIFs than *GL-FEM* even if the crack is not discretized in the global domain.

C. A Multiple Site Damage Problem

A multiple site damage (MSD) example is analyzed in this section. MSD problems focus on the combined effect of multiple growing cracks where each individual crack can be harmless, but the combined effect of several cracks can be disastrous [30]. In this class of problems, cracks cannot

TABLE V: Normalized mode I and II stress intensity factors for the problem shown in Figure 13. Cracks are not discretized in the global domain.

nDOFs	nDOFs	nDOFs	Mode I SIF			Mode II SIF		
(IG)	(L)	(EG)	*GL-FEM*	*GFEM*$^{\text{g-l}}$	Ref.	*GL-FEM*	*GFEM*$^{\text{g-l}}$	Ref.
1080	21240	1134	0.2147	0.5854	0.6013	-0.1280	-0.3003	-0.2910

be treated separately, and the interaction among them must be considered during the analysis. One example of MSD is the case of small fatigue cracks developing around regions with high stress concentrations and manufacturing or material defects. The microcracks may grow and coalesce into a larger macrocrack which can lead to the failure of the structure [31]. The global-local FEM requires sufficiently large local domains in order to minimize the effect of the approximate boundary conditions. In the case of MSD problems this will invariably lead to the inclusion of perhaps several microcracks in the local problems, offsetting some of the advantages of the method. In this section, we analyze the MSD problem shown in Figure 15 using both the *GL-FEM* and the *GFEM*$^{\text{g-l}}$. This problem was originally proposed in [32]. We investigate the effect of the local domain size on the quality of the energy release rate extracted from *GL-FEM* and *GFEM*$^{\text{g-l}}$ solutions.

In the example shown in Figure 15 there are two small MSD cracks on the left and right sides of the main crack. The modeling of the MSD cracks in the global domain would require extremely fine meshes leading to a large global problem. The following parameters are assumed in the simulations: Poisson's ratio $\nu = 0.33$; Young's modulus $E = 10,500$ ksi; in-plane dimensions $d = 75.0$ in, $c = 45.0$ in, $a_1 = 20.0$ in, $a_2 = 11.5$ in, $a_3 = 2.0$ in; size of MSD cracks $a_4 = 1.0$ in; domain thickness $t = 1.0$ in; vertical traction $t_y = 20.0$. We take advantage of symmetry in geometry and boundary conditions and model only the right half (CDEFG) of the domain.

The energy release rate ($\mathscr{G}$) is computed at the center of the front of the main crack, i.e., at $z = t/2$. Plane strain conditions are assumed at this location and the energy release rate is computed using the relation

$$\mathscr{G} = \frac{1-\nu^2}{E} K_I^2 + \frac{1-\nu^2}{E} K_{II}^2 + \frac{1+\nu}{E} K_{III}^2 \tag{9}$$

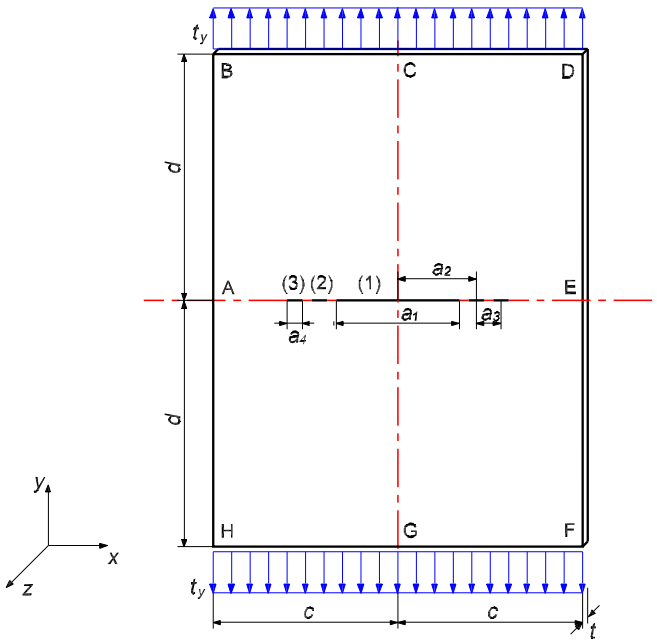

FIG. 15: Description of a multisite damage problem.

where ν is Poisson's ratio, and E is Young's modulus. The stress intensity factors K_I, K_{II} and K_{III} are extracted using the contour integral method [27–29, 33, 34]. The reference value for the $\mathscr{G}$ is taken as 2.5609. This value was computed using a very refined mesh and high order shape functions ($p = 4$) with all cracks modeled in the global problem. This reference discretization has a total of 365,538 degrees of freedom. We checked the convergence of the computed reference value for $\mathscr{G}$ by solving the problem using a smaller model, with 311,742 degrees of freedom. The difference in the energy release rates between these two models was less than 0.01 %.

The discretizations shown in Figure 16 are used in the analysis presented below. Local domains of different sizes are used as illustrated in Figure 16(a). Only the main crack is discretized in the global problem. The neighborhood of the main crack front and the entire MSD cracks are modeled in the local domains (Cf. Figures 16(a) and 16(b)). Not modeling the MSD cracks in the global domain considerably reduces the computational cost and also facilitates the creation of the macroscale discretization. In the case of the $GFEM^{g\text{-}l}$, the local solutions are used to enrich the global nodes illustrated in Figure 16(c). The same set of 12 nodes is enriched, regardless of the

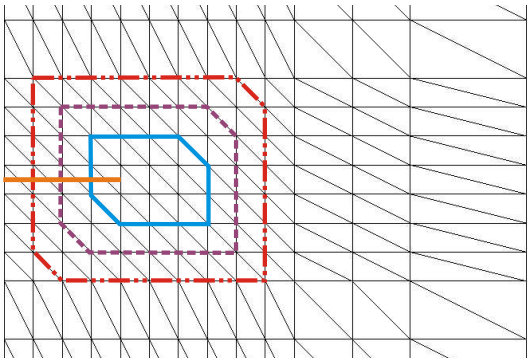

(a)Discretization of cracks in the initial global problem. Solid, dashed and long dash-double dotted lines represent the boundaries of local domains with three different sizes used in this analysis.

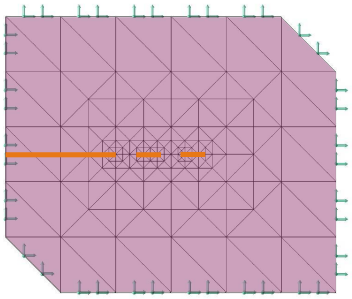

(b)Graded mesh used in the discretization of the local problem represented by a dashed line in Figure 16(a)

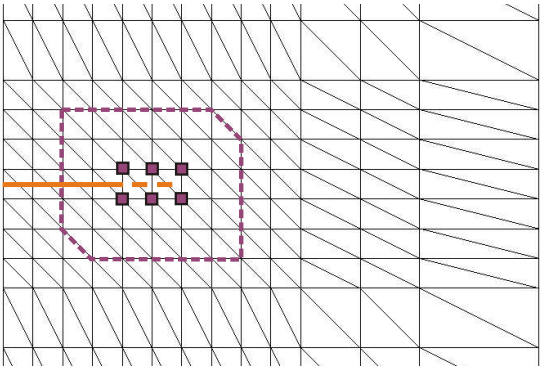

(c)Enrichment of global discretization with the local solution in Figure 16(b). Global nodes enriched with the local solution are represented by squares.

FIG. 16: Discretization of the MSD problem (front view). *Only the main crack is discretized in the global domain* while both the main and MSD cracks are discretized in the local domains.

size of local domain.

The local meshes are strongly refined in the neighborhood of the crack fronts. Singular Westergaard functions are used in local elements intersecting a crack front. Cubic shape functions are used in the initial and enriched global problems and in the local problems as well.

Table VI lists the energy release rate ($\mathscr{G}$) extracted from *GL-FEM* and *GFEM*$^{\text{g-l}}$ solutions for varying sizes of local domains. In the table, the three different sizes of local domains illustrated

TABLE VI: Energy release rate ($\mathscr{G}$) extracted from *GL-FEM* and *GFEM*$^{g\text{-}l}$ solutions for varying sizes of local domains. Rel. err. stands for relative error of extracted $\mathscr{G}$.

Size of	nDOFs	nDOFs	nDOFs	*GL-FEM*		*GFEM*$^{g\text{-}l}$	
Local Domain	(IG)	(L)	(EG)	$\mathscr{G}$	Rel. err. (%)	$\mathscr{G}$	Rel. err. (%)
Small	17280	40662	17316	1.9630	23.35	2.4706	3.53
Middle	17280	40662	17316	2.1566	15.79	2.4828	3.05
Large	17280	40662	17316	2.2783	11.04	2.4942	2.60
Ref.	365538			2.5609		2.5609	

in Figure 16(a) are denoted by “small”, “middle” and “large”. The results show that, for all sizes of local problems used, the energy release rate computed by the *GFEM*$^{g\text{-}l}$ is more accurate than in the case of the *GL-FEM*. The relative error in $\mathscr{G}$ computed with the *GL-FEM* is about six times greater than the one by *GFEM*$^{g\text{-}l}$ when the “small” local domain is used, and four times greater for the “large” local domain. This demonstrates, again, that the *GFEM*$^{g\text{-}l}$ is more robust and accurate than the *GL-FEM*.

The deformed shape of the global domain before and after enrichment with the local solution is displayed in Figure 17. The opening of the small MSD cracks can be clearly captured in the global domain after the enrichment with the local solution, as shown in Figure 17(b), although they are represented only in the local problem.

V. SUMMARY AND CONCLUDING REMARKS

In this paper, we have compared the effectiveness of the global-local approach used in the FEM with the GFEM with global-local enrichment functions presented in [8, 9]. Our focus is on problems involving interacting macrocracks as well as interactions among cracks with different scale sizes. The numerical experiments presented in this paper show that the *GFEM*$^{g\text{-}l}$ is much more robust than the *GL-FEM*. Specifically, the following observations regarding the robustness of the methods can be made:

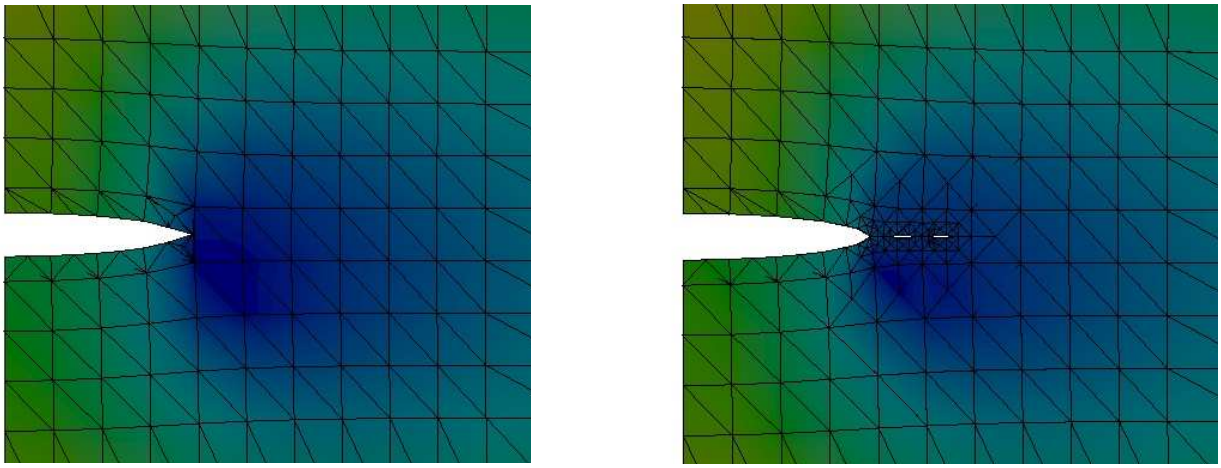

(a)Deformed shape of the global domain before enrichment with a local solution.

(b)Deformed shape of the global domain after enrichment with a local solution.

FIG. 17: Deformed shape of the global domain in the MSD problem before and after enrichment with a local solution. The elements of the local problem nested in the global mesh are visualized in Figure 17(b).

- The numerical examples presented in Section IV A show that the *GFEM*$^{g\text{-}l}$ is less sensitive to the quality of boundary conditions applied to the local problems than the *GL-FEM*. Accurate SIFs could be extracted from *GFEM*$^{g\text{-}l}$ solutions even when cracks were not modeled in the global problem. The SIFs extracted from *GL-FEM* solutions showed an error of up to one order of magnitude larger than in the case of the *GFEM*$^{g\text{-}l}$.

- When cracks were modeled in the initial global problems, the quality of SIFs extracted from *GL-FEM* solutions improved significantly with the accuracy of the initial global problem. However, increasing the polynomial order used in the initial global problem did *not* improve the performance of the *GL-FEM* much when cracks were not modeled in the global problem.

- Energy release rates extracted from *GFEM*$^{g\text{-}l}$ solutions of an MSD problem consistently exhibited higher accuracy than in the case of the *GL-FEM* for all sizes of local domains considered in the numerical experiments.

- The *GFEM*$^{g\text{-}l}$ can account for interactions among cracks with the same or different scale sizes, even when not all cracks are modeled in the initial global problem. This makes

the *GFEM*$^{g\text{-}l}$ an appealing method to analyze problems with phenomena spanning multiple spatial scales.

Our work in [9] also shows that the *GFEM*$^{g\text{-}l}$ is computationally very efficient. The cost of the method when analyzing stationary cracks, like in this paper, is very close to the *GL-FEM*, since the cost of solving the enriched global problem is small when compared with the cost for the initial global problem [9]. The cost analysis presented in [9] was done on a single processor machine for the case of a single local problem defined per crack in the domain. Our on-going research shows, however, that the method is also highly scalable and can be parallelized without difficulty. The robustness and computational efficiency of the *GFEM*$^{g\text{-}l}$ makes it suited to the analysis of practical fracture mechanics engineering problems.

Acknowledgments

The partial support of this work by the National Center for Supercomputing Applications and the University of Illinois at Urbana-Champaign, under the auspices of the NCSA/UIUC Faculty Fellows Program, and by the National Science Foundation under grant DMS-0611094 is gratefully acknowledged.

---

[1] M. Kayama and N. Totsuka. Influence of interaction between multiple cracks on stress corrosion crack propagation. *Corrosion Science*, 44:2333–2352, 2002.

[2] M. Kayama and T. Kitamura. A simulation on growth of multiple small cracks under stress corrosion. *International Journal of Fracture*, 130:787–801, 2004.

[3] H. Kebir, J. M. Roelandt, and Chambon L. Dual boundary element method modelling of aircraft structural joints with multiple site damage. *Engineering Fracture Mechanics*, 73:418–434, 2006.

[4] M. Seyedi, S. Taheri, and F. Hild. Numerical modeling of crack propagation and shielding effects in a striping network. *Nuclear engineering and design*, 236:954–964, 2006.

[5] C. A. Felippa. Introduction to finite element methods., 2004. Course Notes. Department of Aerospace Engineeing Sciences, University of Colorado at Boulder. Available at http://www.colorado.edu/engineering/Aerospace/CAS/courses.d/IFEM.d/.

[6] A. K. Noor. Global-local methodologies and their applications to nonlinear analysis. *Finite Elements in Analysis and Design*, 2:333–346, 1986.

[7] A.Th. Diamantoudis and G.N. Labeas. Stress intensity factors of semi-elliptical surface cracks in pressure vessels by global-local finite element methodology. *Engineering Fracture Mechanics*, 72:1299–1312, 2005.

[8] C.A. Duarte, D.-J. Kim, and I. Babuška. Chapter: A global-local approach for the construction of enrichment functions for the generalized fem and its application to three-dimensional cracks. In V.M.A. Leitão, C.J.S. Alves, and C.A. Duarte, editors, *Advances in Meshfree Techniques*, volume 5 of *Computational Methods in Applied Sciences*, The Netherlands, 2007. Springer. ISBN 978-1-4020-6094-6.

[9] C.A. Duarte and D.-J. Kim. Analysis and applications of a generalized finite element method with global-local enrichment functions. *Computer Methods in Applied Mechanics and Engineering*, 2007. Accepted for publication. http://dx.doi.org/10.1016/j.cma.2007.08.017.

[10] M. B. Civelek and F. Erdogan. Crack problems for a rectangular plate and an infinite strip. *International Journal of Fracture*, 19:139–159, 1982.

[11] C. T. Sun and K. M. Mao. A global-local finite element method suitable for parallel computations. *Computers and Structures*, 29:309–315, 1988.

[12] I. Babuška and T. Strouboulis. *The Finite Element Method and its Reliability*. Numerical Mathematics and Scientific Computation. Oxford Science Publications, New York, USA, 2001.

[13] I. Babuška and J. M. Melenk. The partition of unity finite element method. *International Journal for Numerical Methods in Engineering*, 40:727–758, 1997.

[14] C.A. Duarte, I. Babuška, and J.T. Oden. Generalized finite element methods for three dimensional structural mechanics problems. *Computers and Structures*, 77:215–232, 2000.

[15] J.T. Oden, C.A. Duarte, and O.C. Zienkiewicz. A new cloud-based *hp* finite element method. *Computer Methods in Applied Mechanics and Engineering*, 153:117–126, 1998.

[16] T. Strouboulis, K. Copps, and I. Babuška. The generalized finite element method. *Computer Methods*

in Applied Mechanics and Engineering, 190:4081–4193, 2001.

[17] C.A. Duarte, D.-J. Kim, and D.M. Quaresma. Arbitrarily smooth generalized finite element approximations. *Computer Methods in Applied Mechanics and Engineering*, 196:33–56, 2006. http://dx.doi.org/10.1016/j.cma.2005.12.016.

[18] J.T. Oden and C.A. Duarte. Chapter: Clouds, Cracks and FEM's. In B.D. Reddy, editor, *Recent Developments in Computational and Applied Mechanics*, pages 302–321, Barcelona, Spain, 1997. International Center for Numerical Methods in Engineering, CIMNE.

[19] J.T. Oden and C.A.M. Duarte. Chapter: Solution of singular problems using *hp* clouds. In J.R. Whiteman, editor, *The Mathematics of Finite Elements and Applications– Highlights 1996*, pages 35–54, New York, NY, 1997. John Wiley & Sons.

[20] C.A. Duarte, O.N. Hamzeh, T.J. Liszka, and W.W. Tworzydlo. A generalized finite element method for the simulation of three-dimensional dynamic crack propagation. *Computer Methods in Applied Mechanics and Engineering*, 190:2227–2262, 2001. http://dx.doi.org/10.1016/S0045-7825(00)00233-4.

[21] N. Moes, J. Dolbow, and T. Belytschko. A finite element method for crack growth without remeshing. *International Journal for Numerical Methods in Engineering*, 46:131–150, 1999.

[22] N. Sukumar, N. Moes, B. Moran, and T. Belytschko. Extended finite element method for three-dimensional crack modelling. *International Journal for Numerical Methods in Engineering*, 48(11):1549–1570, 2000.

[23] G. N. Wells and L. J. Sluys. A new method for modeling cohesive cracks using finite elements. *International Journal for Numerical Methods in Engineering*, 50:2667–2682, 2001.

[24] A. Simone. Partition of unity-based discontinuous elements for interface phenomena: Computational issues. *Communications in Numerical Methods in Engineering*, 20:465–478, 2004.

[25] C.A. Duarte, L.G. Reno, and A. Simone. A high-order generalized FEM for through-the-thickness branched cracks. *International Journal for Numerical Methods in Engineering*, 72(3):325–351, 2007. http://dx.doi.org/10.1002/nme.2012.

[26] T. Strouboulis, L. Zhang, and I. Babuška. Generalized finite element method using mesh-based handbooks: Application to problems in domains with many voids. *Computer Methods in Applied Mechanics and Engineering*, 192:3109–3161, 2003.

[27] B. A. Szabo and I. Babuška. Computation of the amplitude of stress singular terms for cracks and

reentrant corners. In T. A. Cruse, editor, *Fracture Mechanics: Nineteenth Symposium, ASTM STP 969*, pages 101–124, 1988.

[28] J.P. Pereira and C.A. Duarte. Extraction of stress intensity factors from generalized finite element solutions. *Engineering Analysis with Boundary Elements*, 29:397–413, 2005.

[29] J.P. Pereira and C.A. Duarte. Computation of stress intensity factors for pressurized cracks using the generalized finite element method and superconvergent extraction techniques. In P.R.M. Lyra, S.M.B.A. da Silva, F.S. Magnani, L.J. do N. Guimaraes, L.M. da Costa, and E. Parente Junior, editors, *XXV Iberian Latin-American Congress on Computational Methods in Engineering*, Recife, PE, Brazil, November 2004. 15 pages. ISBN Proceedings CD: 857 409 869-8.

[30] I. Babuška and B. Andersson. The splitting method as a tool for multiple damage analysis. *SIAM journal on scientific computing*, 26:1114–1145, 2005.

[31] A. Yohannes, D. J. Cartwright, and R. A. Collins. Application of a discontinuous strip yield model to multiple site damage in stiffened sheets. In *The 1996 4th International Conference on Computer-Aided Assesment and Control*, pages 565–572, Fukuoka; Japan, 1996.

[32] L. Wang, F. W. Brust, and S. N. Atluri. The elastic-plastic finite element alternating method(EPFEAM) and the prediction of fracture under WFD conditions in aircraft structures. *Computational Mechanics*, 19:356–369, 1997.

[33] M. Stern, E. B. Becker, and R. S. Dunham. A contour integral computation of mixed-mode stress intensity factors. *International Journal of Fracture*, 12:359–368, 1976.

[34] J.P. Pereira and C.A. Duarte. The contour integral method for loaded cracks. *Communications in Numerical Methods in Engineering*, 22(5):421–432, 2006. http://dx.doi.org/10.1002/cnm.824.

List of Tables

List of Figures